

# A Validated Model for a Pin-Slot Clearance Joint

Luka Skrinjar<sup>1</sup>, Janko Slavič<sup>2</sup>, Miha Boltežar<sup>2</sup>

<sup>1</sup>ETI Elektroelement d. d., Obrezija 5, 1411 Izlake, Slovenia

<sup>2</sup>Faculty of Mechanical Engineering, University of Ljubljana, Slovenia

December 3, 2016

## Abstract

Cite as:

Luka Skrinjar, Janko Slavič and Miha Boltežar

**A Validated Model for a Pin-Slot Clearance Joint**

**Nonlinear Dynamics**, available online: 30 November 2016

DOI: 10.1007/s11071-016-3234-y, free access: [rdcu.be/m8nY](http://rdcu.be/m8nY)

The numerical modeling of joints with a certain amount of clearance and a subsequent validation of the model are important for accurate multi-body simulations. For such validated modeling, not only the kinematic constraints, but also the contact models, are important.

If a joint has no clearance, it is assumed to be ideal. However, in real applications there is frequently some clearance in the joints. Adding clearance and kinematic conditions to a pin-slot joint significantly increases the number of kinematic and contact parameters. Consequently, the resulting kinematics and the contact forces can vary significantly with regards to the selection of those parameters.

This research covers the development of a validated model for a pin-slot clearance joint. Different kinematic constraints and contact models are discussed. The presented model is an experimentally validated one for a pin-slot clearance joint that is commonly used in safety-critical applications like electrical circuit breakers. Special attention is given to the Hertz, Kelvin-Voigt, Johnson and Lankarani-Nikravesh contact models.

When comparing different contact models within numerical approaches and comparing the results with experimental data, significant differences in the results were observed. With a validated model of a pin-slot clearance joint a physically consistent numerical simulation was obtained.

*Keywords* clearance joints, multibody dynamics, contact models, measured impact forces

## 1 Introduction

In the design process for mechanical assemblies, corresponding mechanical joints have to be used to achieve the full functionality of the product. In the theory of multibody dynamics [1, 2] these mechanical joints are modeled as kinematic constraints. A frequently used, planar mechanical joint in engineering applications is the slide contact with clearance, also known as the pin-slot clearance joint. For a validated dynamic response, the dynamic models must include physically consistent kinematic constraints [1, 3]. Typically, these kinematic constraints are modeled without including imperfections [4, 5] (e.g., friction, clearance, wear or lubricant). For the sake of completeness, the following paragraphs discuss current approaches to the clearance in the kinematic constraints, the types of kinematic constraints, the contact models and the friction models.

Clearance in kinematic constraints is typically approached using the continuous approach [6] or the non-smooth dynamics formulation [7]. The penalty method is the most frequently used continuous approach, where contact forces and deformations are modeled with a set of spring-damper elements that represent the surface compliance of the contact bodies [8]. In the non-smooth approach, the unilateral constraints are solved as a linear complementary problem (LCP) [9, 10]. Which approach is more appropriate, depends on the type of problem to be solved [11].

The joint constraints are introduced to the system of differential equations as a set of algebraic equations. The most commonly used and researched constraint with clearance is the revolute joint [12], while the clearance in a prismatic joint is less researched [5]. In revolute joints, several studies focus on the clearance. Pereira et al. modeled the dynamics of chain drives with an included roller-sprocket and bushing-sprocket contact [13], and they used an enhanced

cylindrical contact model [14]. In the research of Gummer and Sauer [15] an overview of a variety of investigated slider-crank mechanisms is presented; the clearance in the revolute joint was simulated with the commercial software RecurDyn. The influence of clearance in the pin-bushing type of revolute joint on the dynamics of a partly compliant mechanism was studied numerically and experimentally by Erkaya et al. [16]. The researchers Xu and Qi et al. used the idea to model a revolute clearance joint as two colliding bodies in an analysis of a multibody system with rolling ball bearings [17] and [18]. In the research [19] of Xu and Yang localized defects were included in the model of a rolling ball bearing. The clearance effect in prismatic joints was investigated by Zhuang and Wang in [20] where the components were assumed to be rigid, while in [21] the slider was considered to be deformable and modeled using the finite-element method (FEM). Kinematic constraints like a cam with a follower were also a research topic [22] using the non-smooth approach. A basic prismatic joint with clearance has infinite length, otherwise it could result in a locked position at some point, if a mechanism has only 1 DOF (like a slider-crank mechanism). To date, much work has been done on clearance in revolute and prismatic constraints, while the pin-slot clearance constraint has not been studied extensively, although it can also be found in engineering applications.

With the continuous approach to modeling the clearance in kinematic constraints, a contact model that best describes the evolution of the contact force during impact has to be selected. The basic contact model was proposed by Hertz [23] and was later further developed by several researchers to include energy dissipation by using a damping coefficient [24]. Contact parameters such as the contact stiffness, which depends on the geometry and the material of the bodies in contact, and the damping coefficient can be evaluated analytically [25, 26] or experimentally [27, 28]. In the revolute clearance joint's contact geometry the contact parameters are constant, while in a pin-slot clearance joint the contact geometry and the parameters depend on the position of a contact point on the slot.

When building kinematic constraints with clearance, besides the contact forces, the friction forces are also important, and they are evaluated with a selected friction model. These models can be classified as static or dynamic

[29]. In static models [30] the friction is modeled as an explicit function of velocity, while in dynamic models the friction depends explicitly on the time, position and velocity [31]. In the research of Askari et al. [32] the friction force, evaluated with a modified version of Coulomb's friction model, is used to predict the wear in a spatial ball joint with clearance.

A nonlinear contact stiffness parameter is used to evaluate the normal contact force; and on the basis of the friction model the wear in the revolute joint with clearance is evaluated [33]. In the majority of problems a dry friction is assumed [21], although in some problems a lubricant effect is modeled in the revolute clearance joint [34]. A Coulomb friction model was used to evaluate the magnitude of the friction force, as this model is frequently used in contact/impact situations due to its simple implementation. Advanced friction models were found not to be significant in this research. While a friction model is used to evaluate the magnitude of the friction force, its direction depends on the tangent at a contact point between the pin and the slot.

This study introduces a validated model of a pin-slot clearance joint based on a combination of the revolute joint with clearance and the prismatic joint with clearance. The geometry of the pin-slot clearance joint allows two possible positions for the contact point. Then, based on its position a contact force in the normal direction is evaluated with a continuous force contact model according to the contact geometry. A comparison of the contact force vector between the numerical and experimental results is shown. The numerical results of the contact force vector for different kinematic constraints and for the pin-slot clearance joint with different types of contact models are presented.

This research is organized as follows: In Section 2, the formulation and the dynamic equations of motion are presented. The equations of the planar pin-slot clearance joint are derived in Section 3, while the contact and friction forces are introduced in Section 4. The validation of the numerical simulations based on the experiment is presented in Section 5 and discussions are presented in Section 6. The conclusions are summarized in Section 7.

## 2 Equations of motion for multibody systems

A mechanical system is an assembly of rigid and deformable bodies that are connected with imperfect kinematic constraints to achieve the design requirements [35].

For a planar mechanical system with  $n_b$  bodies the equations of motion are represented by a set of  $3 \times n_b$  differential equations augmented with a set of  $n_c$  algebraic equations that represent the constraints [2]:

$$\begin{bmatrix} \mathbf{M} & \mathbf{C}_q^T \\ \mathbf{C}_q & \mathbf{0} \end{bmatrix} \begin{bmatrix} \ddot{\mathbf{q}} \\ \boldsymbol{\lambda} \end{bmatrix} = \begin{bmatrix} \mathbf{Q}_e \\ \mathbf{Q}_d \end{bmatrix} \quad (1)$$

where  $\mathbf{M}$  is the mass matrix of the system. Kinematic constraints are represented as a set of holonomic algebraic constraints [5]; a set of  $n_c$  independent algebraic kinematic constraints  $\mathbf{C}$  can be written as [1]:

$$\mathbf{C}(\mathbf{q}, t) = \mathbf{0}. \quad (2)$$

In Equation (1)  $\mathbf{C}_q$  is a constraint Jacobian matrix. Further,  $\ddot{\mathbf{q}}$  is the vector of accelerations,  $\mathbf{Q}_e$  is the vector of generalized forces that contains all the externally applied forces (including the contact forces developed at the clearance joints),  $\boldsymbol{\lambda}$  is the vector of Lagrange multipliers and  $\mathbf{Q}_d$  is the vector that absorbs all the terms of the acceleration constraint equations that depend only on the velocities.

The positional constraints (2) are included in Equation (1) at the accelerations level and therefore numerical integration violations of the constraint equations can arise [34].

As these constraint violations have a greater impact on stiff systems [5], a stabilization method has to be used. The Baumgarte stabilization method [36] or similar methods [37] are usually applied to keep constraint violations under control. The Baumgarte stabilization method modifies Eq. (1) and proposes the next equation:

$$\begin{bmatrix} \mathbf{M} & \mathbf{C}_q^T \\ \mathbf{C}_q & \mathbf{0} \end{bmatrix} \begin{bmatrix} \ddot{\mathbf{q}} \\ \boldsymbol{\lambda} \end{bmatrix} = \begin{bmatrix} \mathbf{Q}_e \\ \mathbf{Q}_d - 2\alpha(\mathbf{C}_q\dot{\mathbf{q}} + \mathbf{C}_t) - \beta^2\mathbf{C} \end{bmatrix}, \quad (3)$$

where the constants  $\alpha$  and  $\beta$  have to be positive to guarantee the stability of the general solution of Eq. (3) [38].

After solving Eq. (1) or (3) for the vectors of the accelerations  $\ddot{\mathbf{q}}$  and the Lagrange multipliers  $\boldsymbol{\lambda}$  the system of  $n$  second-order differential equations is written as a set of  $2n$  first-order differential equations [39]. This is done by defining the new vectors  $\mathbf{y}$  and  $\dot{\mathbf{y}}$ , which contain a vector of positions and velocities and a vector of velocities and accelerations of the system, respectively:

$$\mathbf{y} = [\mathbf{q} \quad \dot{\mathbf{q}}] \quad \text{and} \quad \dot{\mathbf{y}} = [\dot{\mathbf{q}} \quad \ddot{\mathbf{q}}] \quad (4)$$

A numerical integration at time  $t$  that evaluates the state variable at the next time  $t + \Delta t$  is carried out as [12]:

$$\dot{\mathbf{y}}(t) \xrightarrow{\int dt} \mathbf{y}(t + \Delta t) \quad (5)$$

This procedure is repeated until the end time of the dynamic analysis is reached.

### 3 Kinematics of the pin-slot clearance joint

The mathematical model for the pin-slot clearance joint is based on the revolute clearance joint [34] and translational clearance joint [5]. The geometric properties of the pin-slot clearance joint are as shown in Fig 1; length of the slot (guide)  $L$ , width of the slot  $W$  and radius of the pin  $R$ .

In an ideal translational joint, only relative translational motion is allowed. Similarly, in an ideal revolute joint, only the relative rotational motion between two connected bodies is allowed. In the pin-slot clearance joint, the relative rotation between the pin and the slot is not constrained, while the relative translational motion is limited with regards to the slot length/width, see Fig. 1.

As discussed in the introduction, one of the most popular and physically consistent approaches is based on the momentum exchange where the contact force of the colliding bodies is evaluated with an appropriate continuous contact force model [24].

The geometry and the contact situations of the pin-slot clearance joint are significantly more demanding when compared to the revolute joint. Figure 2 shows three possible contact situations. Figure 2 a) no contact between the pin and the slot where the pin is in free-flight motion inside the guide. For no contact, no reaction forces are present. In Figure 2 b) the pin is in contact with

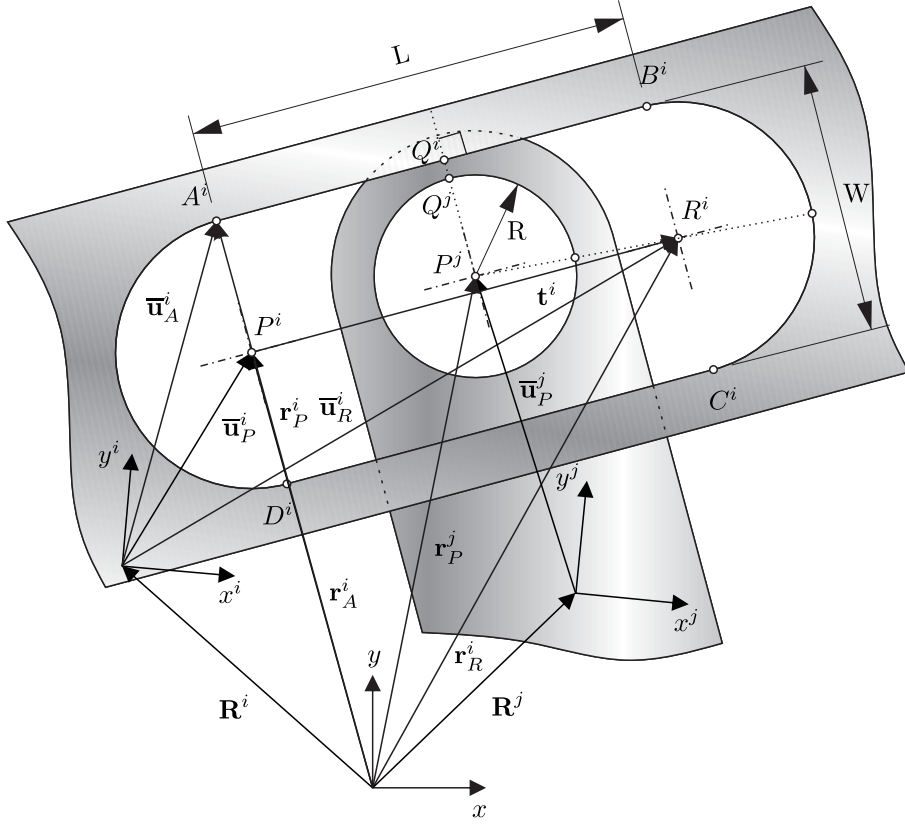


Figure 1: Geometry of the pin-slot clearance joint.

the guide at the straight edge. In Figure 2 c) the pin is in contact with the guide at the cylindrical edge.

Using continuous contact force models the different contact situations are discussed next. Figure 1 shows the pin-slot joint with clearance. The slot is marked as the body  $i$ , while the pin is the body  $j$ . The center of mass of the bodies  $i$  and  $j$  coincides with their local coordinate system, while the  $xy$  coordinate frame represents the inertial coordinate system. The pin body and the slot body are in free flight and are not inertially fixed. Each body can be additionally constrained using kinematic constraint equations, Eq. (2).

The position of a point  $P$  at an arbitrary body  $k = i, j$  in the global coordinate system can be expressed in terms of the absolute coordinates of the body [1]:

$$\mathbf{r}_P^k = \mathbf{R}^k + \mathbf{A}^k \bar{\mathbf{u}}_P^k, \quad k = i, j \quad (6)$$

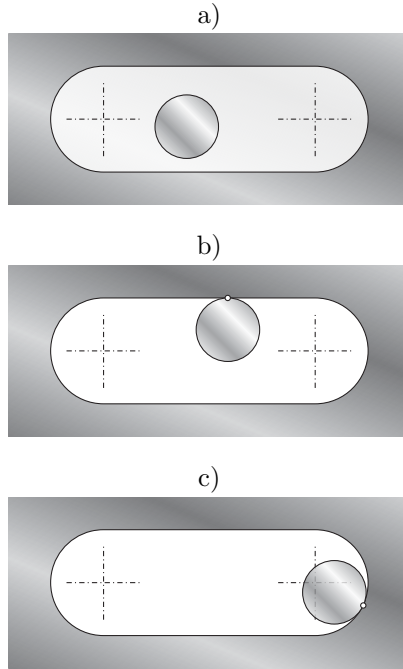


Figure 2: Different contact points between the pin and the slot. a) no contact, b) contact point at the straight edge, c) contact point at the cylindrical edge

where  $\mathbf{R}$  is the absolute position of the center of mass (local coordinate system) in the global coordinate system,  $\bar{\mathbf{u}}$  is the relative position in the local coordinate system, and  $\mathbf{A}$  is a planar transformation matrix.

The velocity of the contact point  $P^k$  can be evaluated by differentiating Eq. (6):

$$\dot{\mathbf{r}}_P^k = \dot{\mathbf{R}}^k + \dot{\mathbf{A}}^k \bar{\mathbf{u}}_P^k, \quad k = i, j \quad (7)$$

The relative normal contact velocity determines whether the bodies are moving towards each other, or away from each other (positive values indicate that the bodies are in the compression phase). The normal and tangential components of the relative contact velocity are determined as [24, 34]:

$$v_n = \mathbf{n}^T (\dot{\mathbf{r}}_j^P - \dot{\mathbf{r}}_i^P) \quad (8)$$

$$v_t = \mathbf{t}^T (\dot{\mathbf{r}}_j^P - \dot{\mathbf{r}}_i^P) \quad (9)$$

where  $\mathbf{n}$  and  $\mathbf{t}$  are the normal and tangent vectors of the contact geometry, respectively, and where subscript  $P$  denotes an actual point of contact that also

defines the normal  $\mathbf{n}$  and tangent  $\mathbf{t}$  vectors.

**Contact point at the straight edge.** In the local coordinate system of body  $i$  the tangent vector  $\bar{\mathbf{t}}^i$  is defined from the point  $P^i$  to the point  $R^i$ :

$$\bar{\mathbf{t}}^i = \bar{\mathbf{u}}_R^i - \bar{\mathbf{u}}_P^i \quad (10)$$

and a tangent in the global coordinate system  $\mathbf{t}$  is defined as:

$$\mathbf{t} = \mathbf{A}^i \bar{\mathbf{t}}^i \quad (11)$$

The contact point can be located on the edge  $A^i B^i$  or  $D^i C^i$ ; in first case the tangent vector is  $\bar{\mathbf{t}}^i$  and in the second, it is  $-\bar{\mathbf{t}}^i$ . The normal vector  $\mathbf{n}$  is obtained by a counter-clockwise rotation ( $\pi/2$ ) of the tangent vector:

$$\mathbf{n} = [t_y, -t_x]^T \quad (12)$$

The distance vector  $d$  of the pin center to the edge of the slot is:

$$\mathbf{d} = (\mathbf{r}_P^j - \mathbf{r}_l^i) - ((\mathbf{r}_P^j - \mathbf{r}_l^i) \mathbf{t}) \mathbf{t}, \quad l = P, R \quad (13)$$

and the length:

$$d = \sqrt{\mathbf{d}^T \mathbf{d}}. \quad (14)$$

Finally, the penetration depth is defined as:

$$\delta = d - R_0^j \quad (15)$$

where  $R_0^j$  is the radius of the pin.

**Contact point at the cylindrical surface.** For a contact point located at the pin and at the cylindrical surface (with center  $P^i$  or  $R^i$ ) the eccentricity vector  $\mathbf{e}$  is defined as [40]:

$$\mathbf{e} = \mathbf{r}_P^j - \mathbf{r}_l^i, \quad l = P, R \quad (16)$$

The length of the eccentricity vector is evaluated as:

$$e = \sqrt{\mathbf{e}^T \mathbf{e}} \quad (17)$$

The normal vector  $\mathbf{n}$  is defined as:

$$\mathbf{n} = \frac{\mathbf{e}}{e} \quad (18)$$

The penetration depth between the pin and the slot is evaluated as:

$$\delta = c - e, \quad (19)$$

where  $c = R_0^j - R_0^i$  is the radial clearance. Similar to the above, the tangent vector obtained with a counter-clockwise rotation ( $\pi/2$ ) of the normal vector:

$$\mathbf{t} = [-n_y, n_x]^T \quad (20)$$

Potential contact points on the bodies  $i$  and  $j$  are  $Q^i$  and  $Q^j$ , as shown in Fig. 1. A simple logic test needs to be implemented to determine the exact position of the pin in the slot and the coordinates of the contact point. Furthermore, the penetration depth is defined with Eq. (15) or (19).

The geometry of the nonparallel edges of a flat section of the slot can also be considered with an additional evaluation of the tangent  $\mathbf{t}^i$  for each flat section of the slot, and the penetration depth at the flat section Eq. (15) can be evaluated per tangent  $\mathbf{t}^i$ . Then, the penetration depth at the cylindrical section Eq. (19) can be evaluated once for every value of radial clearance  $c$  due to the different values of  $R_0^i$  at point  $P^i$  and  $R^i$ .

## 4 Contact forces of the pin-slot with clearance joint

At the contacts between bodies, a contact force model is used to obtain the integrable forces that are included in the equations of motion. These forces are typically in the normal and tangential directions.

**In the normal direction** the Hertz contact model evaluates the contact force as a nonlinear function of the indentation/penetration  $\delta$  [23]:

$$F_n = K\delta^n, \quad (21)$$

where  $K$  is the contact stiffness and  $n$  is the nonlinear power exponent defined by the material and the local geometrical properties of the contacting bodies.

For the contact between two spheres  $i$  and  $j$  with radii  $R_i$  and  $R_j$  the contact stiffness  $K$  is defined as [41]:

$$K = \frac{4}{3(h_i + h_j)} \sqrt{\frac{R_i R_j}{R_i + R_j}} \quad (22)$$

where  $h$  for the body  $k$  is defined as:

$$h_k = \frac{1 - \nu_k^2}{E_k} \quad k = i, j. \quad (23)$$

$E_k$  and  $\nu_k$  represent the Young's modulus and the Poisson's ratio, respectively.

Further details about the contact stiffness  $K$  between a plane and a sphere can be found in [24], and between flat surfaces in [3].

The Hertz contact model (21) does not take into account the dissipation of energy during the contact-impact process and therefore Kelvin and Voigt developed one of the first contact force models that combines a linear spring-damper element in parallel.

When the bodies in contact are moving away from each other, the energy loss is evaluated using the coefficient of restitution [41]:

$$F_n = \begin{cases} K\delta, & \text{if } v_n \geq 0, \\ K\delta c_r, & \text{if } v_n < 0, \end{cases} \quad (24)$$

where  $c_r$  is the coefficient of restitution and  $v_n$  is the relative normal contact velocity, see Equation (8). The Kelvin-Voigt model may not be accurate, as it does not represent the overall nonlinear properties of an impact [24]. A better contact force model is [24]:

$$F_n = K \delta^n + \chi \delta^n \dot{\delta}, \quad (25)$$

where  $\chi$  the hysteresis damping factor. One of the most popular and widely used contact models was introduced by Lankarani and Nikravesh [8]; they defined the hysteresis damping factor as:

$$\chi = \frac{3}{4} \frac{K}{\dot{\delta}_0} (1 - c_r^2). \quad (26)$$

Using Eq. (25), the contact force is:

$$F_n = K \delta^n \left( 1 + \frac{3}{4} \frac{\dot{\delta}}{\dot{\delta}_0} (1 - c_r^2) \right) \quad (27)$$

For the internal contact between the pin and the half-circular end, the Johnson cylindrical contact model [42] can be used. The penetration  $\delta$  is defined as:

$$\delta = \frac{f_n}{\pi E^*} \left( \ln \left( \frac{4\pi E^* \Delta R}{f_n} \right) - 1 \right), \quad (28)$$

where  $f_n$  is the contact force per unit axial length and  $E^*$  is the contact's module of elasticity [42]:

$$\frac{1}{E^*} = \frac{1 - \nu_i^2}{E_i} + \frac{1 - \nu_j^2}{E_j}. \quad (29)$$

$E_i$  and  $E_j$  are the moduli of elasticity for the bodies  $i$  and  $j$ , respectively. Similarly,  $\nu_i$  and  $\nu_j$  are the Poisson's ratios. In Eq. (28),  $\Delta R$  is defined as:

$$\Delta R = R_i \pm R_j \quad (30)$$

where the  $\pm$  sign depends on the contact geometry, being  $(-)$  for the internal and  $(+)$  for the external contact between two cylinders.

Typically, the cylindrical contact models, like (28), represent the indentation  $\delta$  as a nonlinear function of the contact force  $f_n$  [43].

To evaluate the contact force  $f_n$  at each integration time step, an iterative technique is required (e.g., the Newton-Raphson method). Consequently, several researchers tried to avoid the root finding, e.g., based on the Lankarani-Nikravesh and the Johnson models, while Pereira et al. [14] introduced an enhanced cylindrical contact model.

**In the tangential direction** the relative tangential velocity results in tangential friction forces at the contact between two bodies. Several researchers have used a Coulomb friction model to model friction in revolute clearance joints [44, 45, 46]. The most widely employed friction model is the Coulomb friction law [47]:

$$F_t = -\mu F_n \text{sign}(v_t) \quad (31)$$

where  $\mu$  is the coefficient of friction and  $F_n$  is the force in the normal direction. The contact forces that arise in the frictional contact and act on the body  $i$  are:

$$\mathbf{F}^i = F_n \mathbf{n}^i + F_t \mathbf{t}^i \quad (32)$$

and for the body  $j$ :  $\mathbf{F}^j = -\mathbf{F}^i$ . These contact forces are introduced to the system Equations (1) or (3) via the vector of generalized external forces  $\mathbf{Q}_e$ . For an arbitrary planar body  $k$  with the known contact force  $\mathbf{F}^k$  and the position vector  $\bar{\mathbf{u}}_P^k$  (6) the generalized external force is defined as [1]:

$$\mathbf{Q}_e^k = \begin{bmatrix} \mathbf{F}^{kT} \\ \mathbf{F}^{kT} \mathbf{A}_\theta^k \bar{\mathbf{u}}_P^k \end{bmatrix}. \quad (33)$$

The contact deformation is evaluated with Eq. (19) for each cylindrical section and with Eq. (15) for each flat section of the slot. If one of the values of the deformation meets the criteria for a contact, i.e., the deformation  $\delta$  is below the user-defined tolerance  $\delta_{TOL}$ , the deformation is used with a contact model to evaluate the magnitude of the normal contact force. The direction of the normal contact force is defined with Eq. (18) or Eq. (12), based on the position of the contact point (cylindrical or flat section). The magnitude of the tangential friction force is evaluated with a selected Coulomb friction model based on the magnitude of the normal contact force. The direction of the friction force is defined with Eq. (11) for every flat section or Eq. (20) for every cylindrical section. The total contact force on the body  $i$  is evaluated with Eq. (32) and for body  $j$  this vector has the opposite direction. The vector of the generalized contact force for each body  $\mathbf{Q}_e^k$  is then evaluated with Eq. (33) and used to construct the external force vector of the system  $\mathbf{Q}_e$ , Eq. (3). This procedure is implemented inside the contact-analysis procedure within the computational procedure for multibody system dynamics, Fig 3, and it runs each integration time step.

## 5 Model validation

A planar mechanical system, specifically designed for this purpose, is researched to validate the pin-slot clearance joint model. The multibody system is assembled from two bodies: a T-shaped aluminum body 0 with a slot and an aluminum pin, body 1, fixed to the ground and connected to the body 0 via a pin-slot clearance joint. The aluminum body 0 is also attached to a pre-stressed helical steel spring, see Fig. 4.

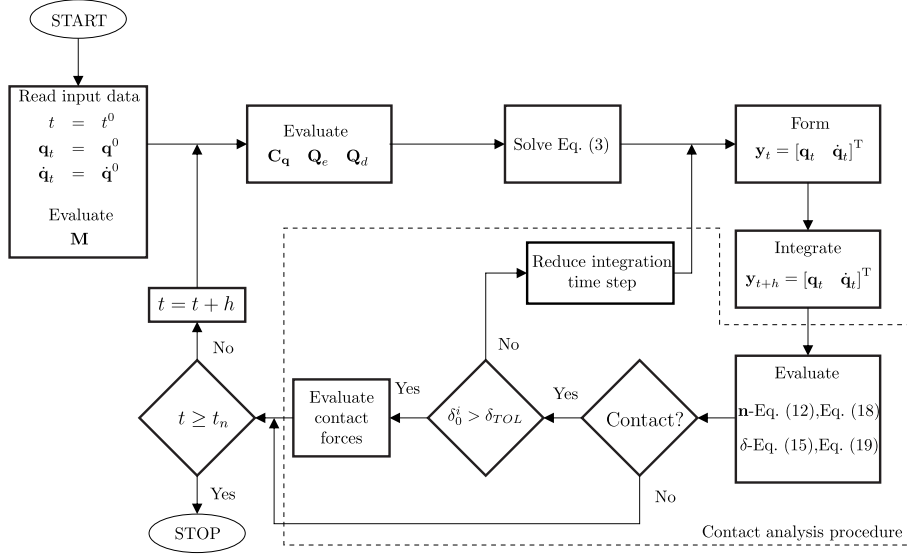


Figure 3: Representation of the computational procedure.

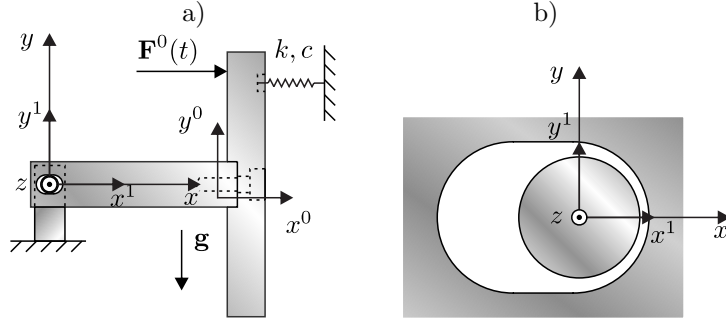


Figure 4: Multibody system with a pin-slot clearance joint

## 5.1 Experimental setup

The experimental setup is shown in Fig. 5 and the sketch of the experimental setup is shown in Fig. 6. The external force is introduced using a stinger mounted on a *LDS V101* electro-dynamical shaker. The applied force is acquired using a *PCB 208C01* 1-axial force sensor. Additionally, a *Kistler 9317A* 3-axial force sensor was used to acquire the contact forces on body 1. The charge signals from the 3-axial force sensor are amplified and converted to a voltage with a *Brüel&Kjaer Nexus 2692* charge amplifier and a high-pass/low-pass filter set at 1 Hz/100 kHz.

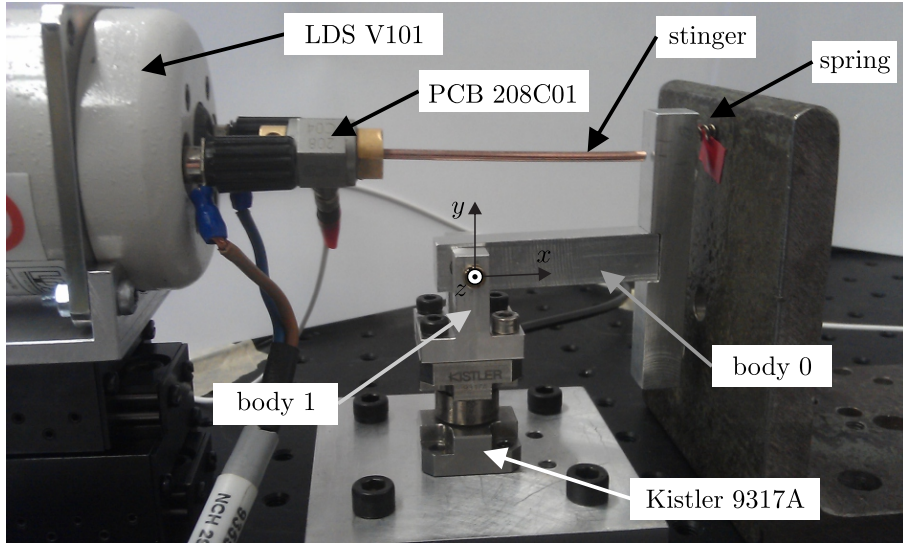


Figure 5: Experimental multibody system with a pin-slot clearance joint

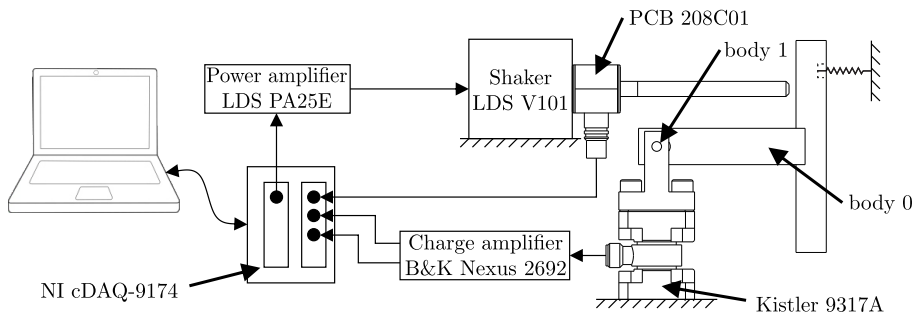


Figure 6: A sketch of a test set-up

The maximum sampling frequency of 51.2 kS/s per channel of the acquisition card *NI 9234* is used to acquire the values of the measured signals and the time between two consecutive acquired values is  $\Delta t = \frac{1}{51200}$  s. The *LDS V101* shaker is controlled with a *NI 9234* output module and the generated signal is amplified with a *LDS PA25E* power amplifier.

## 5.2 Numerical model

Numerical experiments were performed to compare the contact force of the presented pin-slot clearance joint (PSCJ) model with a revolute clearance joint (RCJ) and an ideal revolute joint (IRJ).

An external force vector  $\mathbf{F}^0(t)$  is applied to the body 0 at the location  $\bar{\mathbf{u}}_F^0$  defined in the body's local coordinate system and is modeled as  $\mathbf{F}^0(t) = [F_x^0(t), 0]^T$  where  $F_x^0(t)$  has the form:

$$F_x^0(t) = \begin{cases} F_0 \sin\left(\frac{\pi}{t_F} t\right), & \text{if } t \leq t_F, \\ 0 & \end{cases} \quad (34)$$

and  $F_0$  represents the force amplitude. The inertial frame of reference coincides with the pin body's local coordinate system indexed 1, see Fig 4. The external applied force  $\mathbf{F}^0$  was modeled based on the force impulse of the measurement data so that for the selected time interval  $[0, t_F = 0.0391]$  s the force impulses are equal [48]. A comparison between the measured external force and the modeled force is presented in Fig 7. The experimental values represent the external force that is present when a stinger, mounted on a shaker, impacts with a body 0 slot. To remove the noise and high-frequency structural dynamics, a central moving average of 301 acquired points ( $\Delta T = 301 \cdot \frac{1}{51200} \approx 6$  ms) was used on the experimental and numerical results [49].

Table 1 shows the mass and inertia properties of the bodies for different types of kinematic constraint (PSCJ, RCJ and IRJ). The geometric properties of the system are listed in Table 2.

Table 1: Mass properties of the multibody system

	PSCJ	RCJ	IRJ
$m^0$ [kg]	$32.54 \cdot 10^{-3}$	$32.74 \cdot 10^{-3}$	$32.74 \cdot 10^{-3}$
$J^0$ [kg m <sup>2</sup> ]	$20.94 \cdot 10^{-6}$	$21.40 \cdot 10^{-6}$	$21.40 \cdot 10^{-6}$
$m^1$ [kg]	$1 \cdot 10^{-3}$	$1 \cdot 10^{-3}$	$1 \cdot 10^{-3}$
$J^1$ [kg m <sup>2</sup> ]	$1 \cdot 10^{-6}$	$1 \cdot 10^{-6}$	$1 \cdot 10^{-6}$

The parts used in the experiment were machined with a CNC milling process, and the defined tolerances for the pin diameter and the slot diameters are  $\pm 0.05$  mm and the geometric tolerance of the flatness of the slot flat section is  $\pm 0.05$ . The measurements confirmed that these values are within the defined values.

The numerical integration procedure of Eq. (3) is started with the defined initial conditions  $\mathbf{q}_0$  as they have a strong impact on the prediction of the

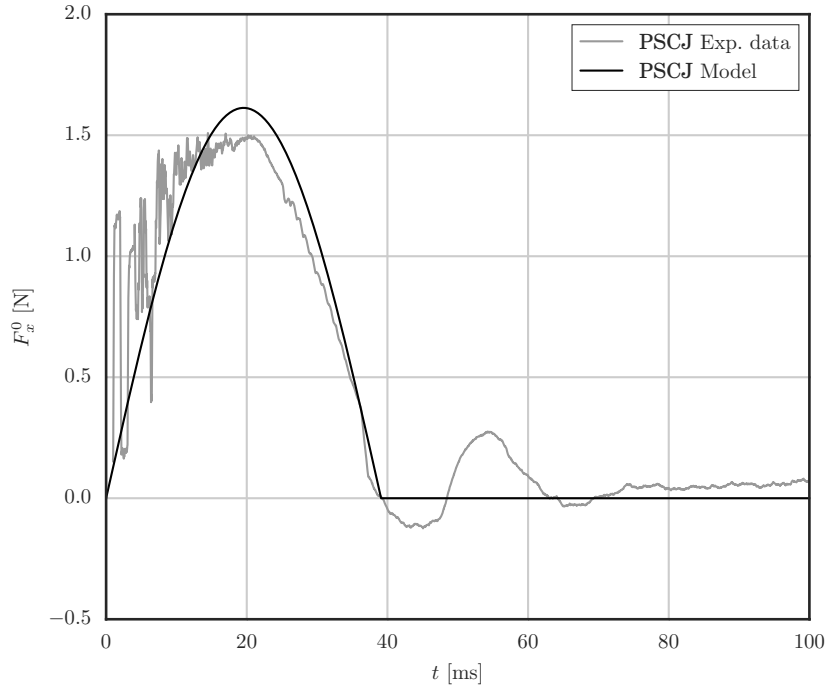


Figure 7: The  $x$ -component of the external force applied to body 0,  $F_x^0$ .

Table 2: Geometrical properties of the multibody system

$[mm]$	PSCJ	RCJ	IRJ
$R_0^0$	/	2.5	/
$R_0^1$	2.45	2.45	/
$L^0$	2	/	/
$h^0$	5	/	/
$\bar{\mathbf{u}}_P^0$	$[-49, 0.0765]$	$[-49, 0.076]$	$[-49, 0.076]$
$\bar{\mathbf{u}}_R^0$	$[-47, 0.0765]$	/	/
$\bar{\mathbf{u}}_P^1$	$[0, 0]$	$[0, 0]$	$[0, 0]$

dynamic performance of mechanical systems [2]. The integration process is performed with the Runge-Kutta-Fehlberg (RKF45) method that has a variable step size and error control [39]. The variable step size is important due to the fact that the time of contact is estimated with sufficient precision and when there

are no contacts present, in the dynamical system, an integration process can use larger time steps to increase the computational efficiency [50]. To ensure the constraint violations are kept under control a Baumgarte stabilization method (BMS) is used [36]. This is implemented within the computational procedure, as presented in Fig 3.

To ensure unwanted energy gains during the time integration when the contact is detected, a contact-detection methodology is implemented, as suggested by Flores and Ambrosio [12]. This methodology ensures that the initial penetration depth  $\delta_0$  is below the user-defined small value and a sufficiently precise time of contact is determined. The key parameters used for the different models are shown in Table 3. These parameters are used to solve the dynamics of the mechanical system.

Table 3: Parameters of the numerical simulation

Width of the slot (contact) $W$ [m]	0.08
Coefficient of restitution $c_r$ [/]	0.4
Kinematic coefficient of friction $\mu_k$ [/]	0.51
Module of elasticity $E$ [GPa]	69
Poisson's ratio $\nu$ [/]	0.35
Integration method	RKF45
BSM parameter $\alpha$ [34]	5
BSM parameter $\beta$ [34]	5
Maximum integration step size $H_{max}$ [s]	$1 \cdot 10^{-4}$
Minimum integration step size $H_{min}$ [s]	$1 \cdot 10^{-12}$
Integration step size during contact $H_{contact}$ [s]	$1 \cdot 10^{-5}$
Simulation end time $t_n$ [s]	$6 \cdot 10^{-2}$
$\delta_0$ [m]	$1 \cdot 10^{-6}$

The contact forces acquired during the experiment for PSCJ are compared with the numerical model for each component in Fig. 8 and Fig. 9. The numerical values of the  $x$  component of the contact force in general show good agreement with the experimental values. One could argue that the experimental and numerical results should match better, but the discussion in the next section will show how much different those result could be in a case where different

kinematic constraints / contact models are employed.

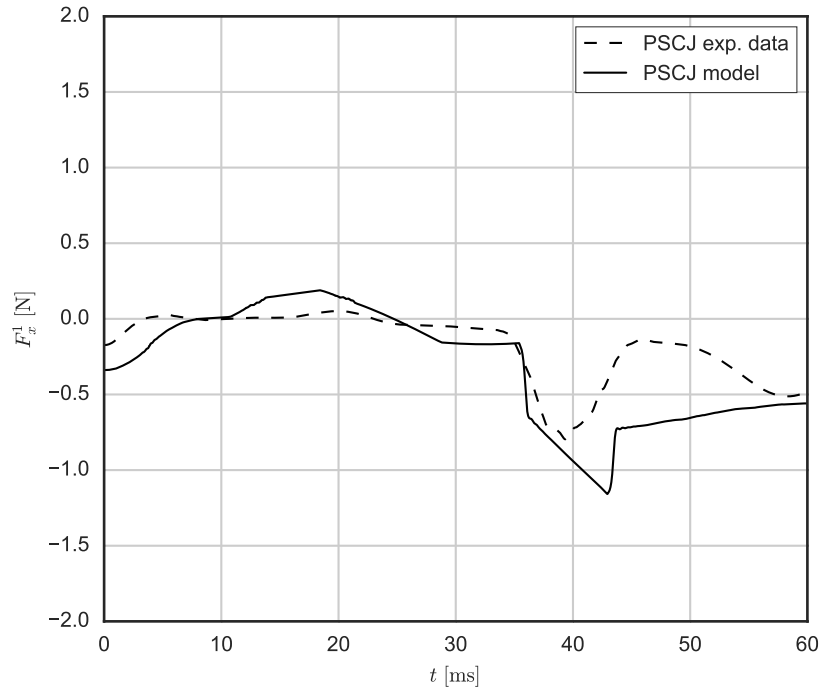


Figure 8: The  $x$  component of the contact force on body 1,  $F_x^1$ , for experimental and numerical data for PSCJ.

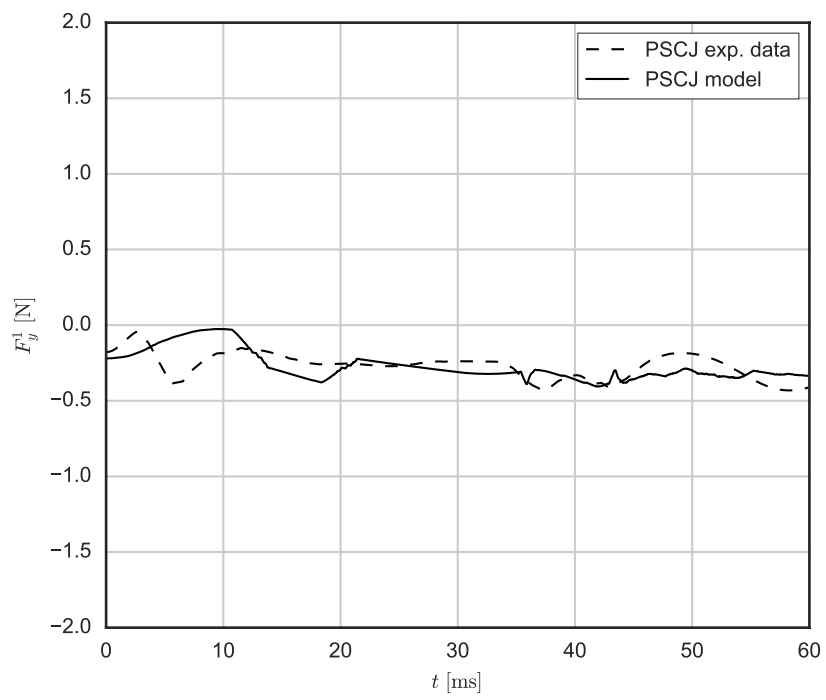


Figure 9: The  $y$  component of the contact force on body 1,  $F_y^1$ , for experimental and numerical data for PSCJ.

## 6 Discussion

In the previous section an experimentally validated numerical model of the pin-slot clearance joint (PSCJ) was presented. Here, the numerical results of PSCJ are compared to an ideal revolute joint (IRJ) and a revolute clearance joint (RCJ).

The contact forces on body 1 in the  $x$  and  $y$  directions are shown in Fig. 10, Fig. 11. From the results it is clear that the RCJ and IRJ would result in significantly different results when compared to the proposed PSCJ joint and the experimental results, see also Figures 8 and 9.

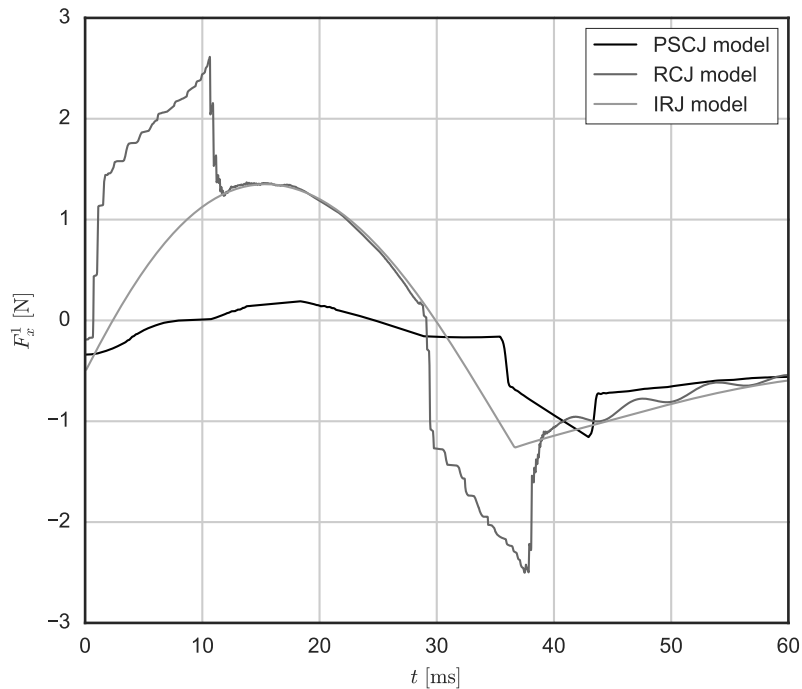


Figure 10: The  $x$  component of the contact force on body 1,  $F_x^1$ , for different kinematic constraints.

Figures 10 and 11 show that different types of joints (with clearance) produce different contact forces: therefore, it is vital to select the appropriate mechanical joint to ensure physical consistency. The RCJ only considers an internal contact between two cylinders, while the PSCJ has two contact options, i.e.,

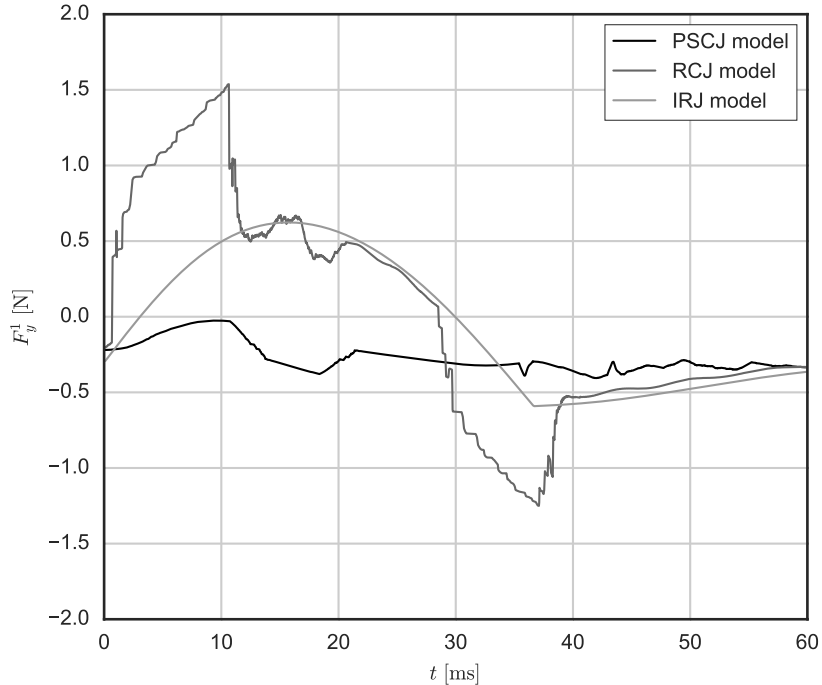


Figure 11: The  $y$  component of the contact force on body 1,  $F_y^1$ , for different kinematic constraints.

the contact between a pin and a cylindrical surface and a contact between a pin and the flat surface of the slot. As presented in Fig. 1 the length of the slot  $L$  enables additional relative movement in the direction of tangent  $\mathbf{t}^i$ . Due to this extra unconstrained movement a contact force has lower values. For these two contact options, different contact parameters also have to be considered (contact stiffness). In the limit case of PSCJ when the value of slot length  $L$  is equal to 0, we obtain a basic RCJ.

With the proposed PSCJ joint a proper contact model is required. As discussed in the introduction, there are several contact models that can be used. Here, only some of them are presented in greater detail: the Hertz, Kelvin-Voigt, Johnson (with and without dissipation) models are compared to the Lankarani-Nikravesh model. The contact forces when different contact models are used with the PSCJ joint are shown in Figures 12 and 13. The Kelvin-Voigt contact model is shown to give the wrong results for this application. The main reason

for this deviation of the numerical results is due to linear dependence of  $F_n$  and  $\delta$ , see Eq. (24), as it does not represent the overall nonlinear nature of an impact [24].

The Johnson and Hertz contact models are closer to the Lankarani-Nikravesh model and the experimental results. Before the final impact, which is at a time around 30 ms, the values of the contact force are similar and the time of impact is longer, while the contact force at the steady state at the end of the movement is larger when the energy dissipation is not considered, especially in the  $x$  direction. The Lankarani-Nikravesh contact model is simple to implement in multibody dynamics code as it introduces an explicit dependence between  $F_n$  and  $\delta$  and also includes hysteresis damping. The problem of evaluating the contact stiffness for the Lankarani-Nikravesh model is solved with the Johnson model. If the experimental results for PSCJ are compared with the contact forces evaluated with the presented approach, based on Lankarani-Nikravesh model, a good agreement can be seen.

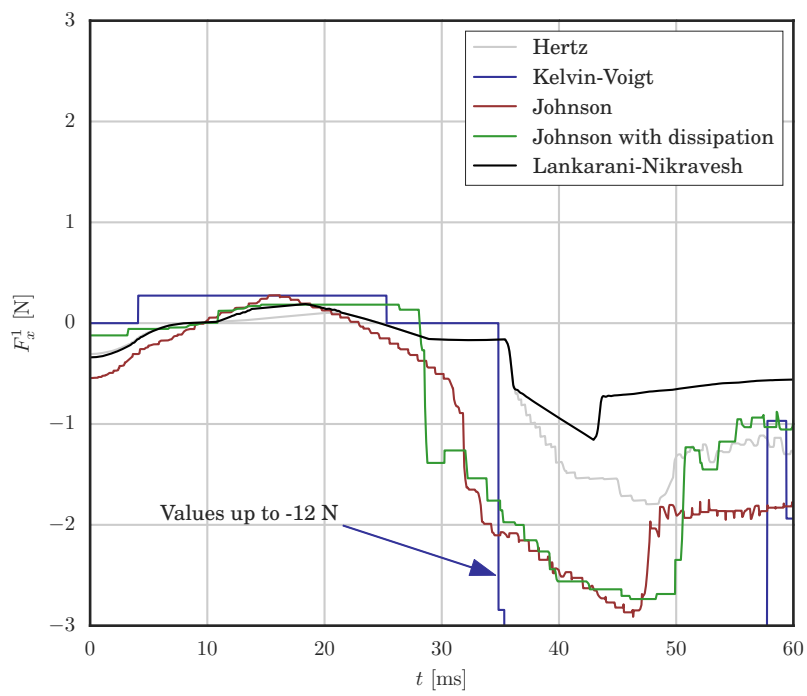


Figure 12: The  $x$  component of the contact force on body 1,  $F_x^1$ , for different contact models.

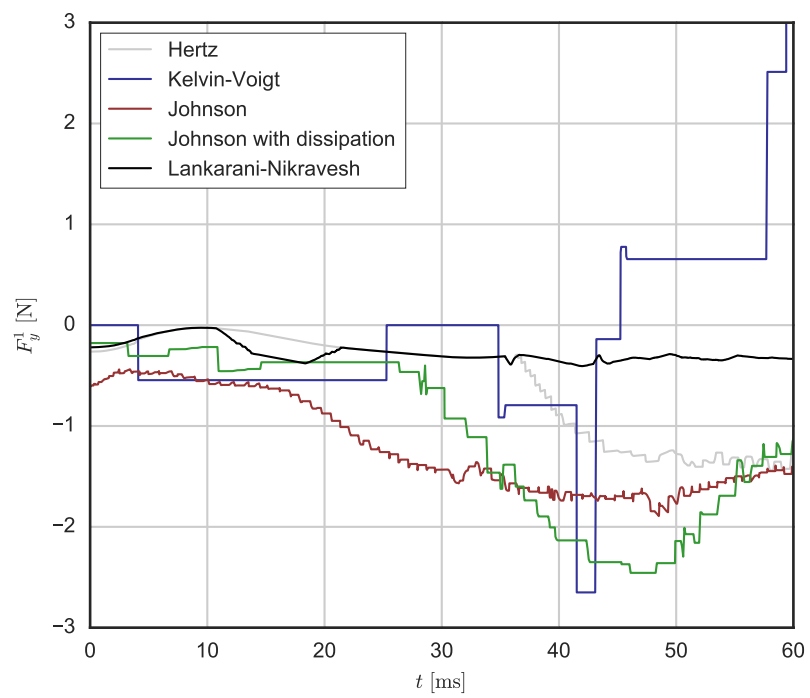


Figure 13: The  $y$  component of the contact force on body 1,  $F_y^1$ , for different contact models.

## 7 Conclusions

In this work a model of a validated pin-slot joint model with clearance is presented. Two possible contact positions between the pin and the slot are shown and the penetration depth is evaluated according to the contact geometry at each contact position. Based on the pin position in the slot different properties of the contact models were used to evaluate the contact forces.

The significance of including the clearance was researched numerically and experimentally. It was found that the proper numerical clearance model results in a similar response to that measured experimentally. However, without the proper modeling of clearance (e.g., pin-joint), the contact forces differ significantly, compared to the experimentally determined forces.

Numerical experiments were performed on a selected multibody system with a pin-slot clearance joint where different contact models were used to evaluate the contact force. The Lankarani-Nikravesh contact model was found to give the best results, when compared to the experimental observations. Other contact models (e.g., Kelvin-Voigt) can result in significantly different contact forces than those measured experimentally .

For the example of a pin-slot clearance joint, this research shows the importance of experimentally validated numerical modeling.

## Acknowledgment

The authors acknowledge the partial financial support of the Slovenian Research Agency (research core funding No. P2-0263)

## References

- [1] Ahmed a. Shabana. *Computational Dynamics 3rd Edition*. 2009.
- [2] Parviz E. Nikravesh. *Planar Multibody Dynamics: Formulation, Programming and Applications*, 2007.
- [3] Parviz E. Nikravesh. *Computer-Aided Analysis of Mechanical Systems*. 1988.

- [4] A. E. H. Love. A Treatise on the Mathematical Theory of Elasticity. *Library*, 1927.
- [5] Flores, Ambrosio, Pimenta, and Lankarani. *Kinematics and Dynamics of Multibody Systems with Imperfect Joints*, volume 34. 2008.
- [6] G Gilardi and I Sharf. Literature survey of contact dynamics modelling. *Mechanism and Machine Theory*, 37(10):1213–1239, 2002.
- [7] F. Pfeiffer. Multibody systems with unilateral constraints. *Journal of Applied Mathematics and Mechanics*, 65(4):665–670, 2001.
- [8] H. M. Lankarani and P. E. Nikravesh. A Contact Force Model With Hysteresis Damping for Impact Analysis of Multibody Systems. *Journal of Mechanical Design*, 112(3):369–376, 1990.
- [9] F. Pfeiffer. Unilateral problems of dynamics. *Archive of Applied Mechanics*, 69(8):503–527, 1999.
- [10] Janko Slavič and Miha Boltežar. Simulating multibody dynamics with rough contact surfaces and run-in wear. *Nonlinear Dynamics*, 45(3-4):353–365, 2006.
- [11] Y a. Khulief. Modeling of Impact in Multibody Systems: An Overview. *Journal of Computational and Nonlinear Dynamics*, 8(2):21012, 2013.
- [12] Paulo Flores and Jorge Ambrosio. On the contact detection for contact-impact analysis in multibody systems. *Multibody System Dynamics*, 24(1):103–122, 2010.
- [13] C. Pereira, J. Ambrósio, and A. Ramalho. Dynamics of chain drives using a generalized revolute clearance joint formulation. *Mechanism and Machine Theory*, 92:64–85, 2015.
- [14] C Pereira, A Ramalho, and J Ambrosio. An enhanced cylindrical contact force model. *Multibody System Dynamics*, 35(3):277–298, 2015.
- [15] A. Gummer and B. Sauer. Modeling planar slider-crank mechanisms with clearance joints in RecurDyn. *Multibody System Dynamics*, pages 127–145, 2012.

- [16] Selçuk Erkaya, Selim Doğan, and Şaban Ulus. Effects of joint clearance on the dynamics of a partly compliant mechanism: Numerical and experimental studies. *Mechanism and Machine Theory*, 88:125–140, 2015.
- [17] L. Xu. A general method for impact dynamic analysis of a planar multibody system with a rolling ball bearing joint. *Nonlinear Dynamics*, 78(2):857–879, 2014.
- [18] Zhaohui Qi, Gang Wang, and Zhigang Zhang. Contact analysis of deep groove ball bearings in multibody systems. *Multibody System Dynamics*, pages 115–141, 2014.
- [19] L. Xu and Y. Yang. Modeling a non-ideal rolling ball bearing joint with localized defects in planar multibody systems. *Multibody System Dynamics*, pages 409–426, 2015.
- [20] F. Zhuang and Q. Wang. Modeling and simulation of the nonsmooth planar rigid multibody systems with frictional translational joints. *Multibody System Dynamics*, 29(4):403–423, 2013.
- [21] Jie Zhang and Qi Wang. Modeling and simulation of a frictional translational joint with a flexible slider and clearance. *Multibody System Dynamics*, pages 1–23, 2015.
- [22] Paulo Flores, Remco Leine, and Christoph Glocker. Application of the nonsmooth dynamics approach to model and analysis of the contact-impact events in cam-follower systems. *Nonlinear Dynamics*, 69(4):2117–2133, 2012.
- [23] Heinrich Hertz. Ueber die Beruehrung fester elastischer Koerper. *Journal fuer die reine und angewandte Mathematik*, 91:156–171, 1881.
- [24] Margarida Machado, Pedro Moreira, Paulo Flores, and Hamid M. Lankarani. Compliant contact force models in multibody dynamics: Evolution of the Hertz contact theory. *Mechanism and Machine Theory*, 53(0):99–121, 2012.

- [25] Jorge Ambrosio and Paulo Verissimo. Improved bushing models for general multibody systems and vehicle dynamics. *Multibody System Dynamics*, 22(4):341–365, 2009.
- [26] H M Lankarani. Canonical Equations of Motion and Estimation of Parameters in the Analysis of Impact Problems. *Department of Aerospace and Mechanical Engineering*, 1988.
- [27] Hossein Barikloo and Ebrahim Ahmadi. Dynamic Properties of Golden Delicious and Red Delicious Apple under Normal Contact Force Models. *Journal of Texture Studies*, 44(6):409–417, 2013.
- [28] S. Baglioni, F. Cianetti, C. Braccesi, and D.M. De Micheli. Multibody modelling of N DOF robot arm assigned to milling manufacturing. Dynamic analysis and position errors evaluation. *Journal of Mechanical Science and Technology*, 30(1):405–420, 2016.
- [29] Henrik Olsson. Control Systems with Friction. *Department of Automatic Control, Lund Institute of Technology*, 1045(October):172, 1996.
- [30] C S Koshy, P Flores, and H M Lankarani. Study of the effect of contact force model on the dynamic response of mechanical systems with dry clearance joints: computational and experimental approaches. *Nonlinear Dynamics*, 73(1-2):325–338, 2013.
- [31] Onesmus Muvengi, John Kihuu, and Bernard Ikua. Dynamic analysis of planar multi-body systems with LuGre friction at differently located revolute clearance joints. *Multibody System Dynamics*, 28(4):369–393, 2012.
- [32] Ehsan Askari, Paulo Flores, Danè Dabirrahmani, and Richard Appleyard. Dynamic modeling and analysis of wear in spatial hard-on-hard couple hip replacements using multibody systems methodologies. *Nonlinear Dynamics*, 82(1-2):1039–1058, 2015.
- [33] W. Xiang, S. Yan, and J. Wu. A comprehensive method for joint wear prediction in planar mechanical systems with clearances considering complex contact conditions. *Science China Technological Sciences*, 58(1):86–96, 2015.

- [34] Paulo Flores, Jorge Ambrosio, and J. Pimenta Claro. Dynamic analysis for planar multibody mechanical systems with lubricated joints. *Multibody System Dynamics*, 12(1):47–74, 2004.
- [35] A A Shabana. *Dynamics of Multibody Systems*. Cambridge University Press, 2005.
- [36] J Baumgarte. Stabilization of constraints and integrals of motion in dynamical systems. *Computer Methods in Applied Mechanics and Engineering*, 1(1):1–16, 1972.
- [37] J. Ambrósio. Impact of Rigid and Flexible Multibody Systems: Deformation Description and Contact Models. pages 57–81, 2003.
- [38] Paulo Flores, Margarida Machado, Eurico Seabra, and Miguel Tavares da Silva. A Parametric Study on the Baumgarte Stabilization Method for Forward Dynamics of Constrained Multibody Systems. *Journal of Computational and Nonlinear Dynamics*, 6(1):011019, 2011.
- [39] Richard L. Burden and John Douglas Faires. *Numerical Analysis*. 2011.
- [40] P. Flores and J. Ambrosio. Revolute joints with clearance in multibody systems. *Computers and Structures*, 82(17-19):1359–1369, 2004.
- [41] W Goldsmith. *Impact: The Theory and Physical Behaviour of Colliding Solids*. Edward Arnold, 1960.
- [42] K L Johnson. *Contact Mechanics*. Cambridge University Press, London, 1995.
- [43] Cândida M. Pereira, Amílcar L. Ramalho, and Jorge A.C. Ambrosio. A critical overview of internal and external cylinder contact force models. *Nonlinear Dynamics*, 63:681–697, 2011.
- [44] Peter Ravn. A Continuous Analysis Method for Planar Multibody Systems with Joint Clearance. *Multibody System Dynamics*, 2(1):1–24, 1998.
- [45] Saad Mukras, Nam H Kim, Nathan A Mauntler, Tony L Schmitz, and W Gregory Sawyer. Analysis of planar multibody systems with revolute joint wear. *Wear*, 268(5–6):643–652, 2010.

- [46] J. Chunmei, Q. Yang, F. Ling, and Z. Ling. The Non-Linear Dynamic Behavior of an Elastic Linkage Mechanism With Clearances. *Journal of Sound and Vibration*, 249(2):213–226, 2002.
- [47] C.A. Coulomb. Theories of simple machines. *Memoires deMath. Phys. Acad. Sci.*, 10:161–331, 1785.
- [48] Thomas R Kane and David a Levinson. Dynamics Theory and Applications. page 402, 1985.
- [49] Steven W. Smith. *Digital Signal Processing*.
- [50] J Slavič and M Boltežar. Non-linearity and non-smoothness in multi-body dynamics: application to woodpecker toy. *Proceedings of the Institution of Mechanical Engineers, Part C: Journal of Mechanical Engineering Science*, 220(3):285–296, 2006.